Sensors and Materials, Vol. 38, No. 2 (2026) 673–678
MYU Tokyo

S & M 4336

Synthesis of Composite Films in Tb_2O_3–Al_2O_3 Eutectic System by CVD method and Their Tb^{3+}-centered Luminescence

Natsumi Imai and Akihiko Ito*

Graduate School of Environment and Information Sciences, Yokohama National University,
79-7 Tokiwadai, Hodogaya-ku, Yokohama, Kanagawa 240-8501, Japan

(Received October 31, 2025; accepted December 22, 2025)

Keywords: Tb_2O_3–Al_2O_3 eutectic system, composite, chemical vapor deposition, luminescence

Composite films in the Tb_2O_3–Al_2O_3 eutectic system were synthesized on sapphire substrates by the laser-assisted chemical vapor deposition method. On a *c*-cut sapphire substrate, $TbAlO_3$ (TAP)–α-Al_2O_3 and $Tb_3Al_5O_{12}$ (TAG)–α-Al_2O_3 composite films were obtained at 6.4–39.6 mol%Tb_2O_3 in precursor vapor. At compositions close to the eutectic point of 22.0 mol%Tb_2O_3, a lamellar structure formed, whereas at compositions far from the eutectic point, a rod-like structure formed. Both TAP–α-Al_2O_3 and TAG–α-Al_2O_3 composite films exhibited green luminescence originating from the $^5D_4$–^7F_n (n = 3–6) transitions of Tb^{3+} centers with decay time constants of 0.67 and 1.46 ms for the TAP–α-Al_2O_3 composite film and 0.75 and 1.31 ms for the TAG–α-Al_2O_3 composite film.

1. Introduction

Directionally solidified eutectics are composite materials in which two or more solid phases precipitate simultaneously from the melt. Eutectics based on the α-Al_2O_3 phase have been studied since the 1990s as high-temperature structural materials for aerospace applications, owing to their excellent strength and thermal stability at high temperatures.[1–3] In the RE_2O_3–Al_2O_3 eutectic system (RE = rare-earth element), REAP (rare-earth aluminum perovskite, $REAlO_3$)–α-Al_2O_3 eutectics were obtained for RE = Sm–Gd, Y, whereas REAG (rare-earth aluminum garnet, $RE_3Al_5O_{12}$)–α-Al_2O_3 eutectics were obtained for RE = Tb–Lu, Y.[4]

By introducing luminescent centers as dopants into REAG and REAP, eutectics can be applicable as phosphors. Ce^{3+}-doped YAG exhibits yellow luminescence,[5] and thus, Ce^{3+}-doped YAG–α-Al_2O_3 eutectics excited by a blue LED has been studied for white LED application.[6,7] Structural advantages have also been reported for GAP–α-Al_2O_3 eutectics, because emission light propagates within the matrix via total internal reflection, efficiently guiding scintillation light to the detector.[8–10] Reports on the synthesis of eutectics focusing on the Tb_2O_3–α-Al_2O_3 eutectic are scarce, limited to research on Ce^{3+}-doped $Tb_3Al_5O_{12}$ (TAG)-α-Al_2O_3 eutectics for LED application.[11,12] Tb^{3+} has been widely used as a dopant, whereas

*Corresponding author: e-mail: ito-akihiko-xr@ynu.ac.jp
https://doi.org/10.18494/SAM6091

ISSN 0914-4935
https://myukk.org/

($TbAlO_3$) TAP and TAG contain Tb^{3+} in their crystal structures and exhibit localized luminescence from Tb^{3+} centers.

All these eutectics were synthesized via the melt-solidification process, which often resulted in an inhomogeneous, Chinese script-like microstructure.[13–15] Therefore, new process methods for forming ordered structures are required. Our research group focused on the CVD method, which enables film synthesis at low temperatures. However, conventional thermal CVD methods struggled to form composite films with a two-phase separation structure. By incorporating laser technology into thermal CVD, we have successfully formed composite films with phase-separated structures in pseudo-binary eutectic systems such as ZrO_2–Al_2O_3 and HfO_2–Al_2O_3.[16,17] We have succeeded in synthesizing single-phase and composite films with phase-separated structures in YAG–Al_2O_3 and LuAG–Al_2O_3 systems.[18–20]

The present study extends the LCVD technique to the Tb_2O_3–Al_2O_3 eutectic system. The objective is to analyze the constituent phases and microstructure of the obtained films and evaluate their luminescence properties.

2. Materials and Methods

The laser-assisted CVD apparatus has been described elsewhere.[21] The synthesis conditions follow those of previous studies on α-Al_2O_3–REAG (RE = Lu, Y) composite films.[18,19] Metal-organic compounds of terbium tris(dipivaloylmethanate) (Strem Chemicals, USA) and aluminum tris(acetylacetonate) (Sigma-Aldrich, USA) were maintained at temperatures of 443–473 K and 453 K, respectively, in precursor furnaces. The resultant vapor was transferred to the CVD chamber using Ar as carrier gas, and O_2 gas was separately introduced to the chamber through a double-tubed nozzle. The molar ratios in the precursor vapor were estimated from the mass change in each precursor before and after deposition, and the molar ratios of Tb_2O_3 were determined to be 6.4–39.6 mol%. The total chamber pressure was maintained at 230–250 Pa. The substrates were *m*-, *c*-, *a*-, and *r*-cut sapphire single crystals ($5 \times 5 \times 0.5$ mm^3) polished on both sides. Each substrate was preheated on a heating stage, then irradiated with a CO_2 laser (wavelength: 10.6 μm; maximum laser output: 60 W) through a ZnSe window. The laser irradiation heated all the substrates to 1000–1216 K. The deposition time was 600 s. The phase compositions of the resultant films were determined by X-ray diffraction (XRD; Bruker D2 Phaser, USA). The microstructures were observed by scanning electron microscopy (SEM; JEOL JCM-6000, Japan). The photoluminescence (PL) and PL excitation (PLE) spectra and afterglow decay curves were measured using a fluorescence spectrophotometer (JASCO FP-8300, Japan).

3. Results and Discussion

Figure 1 shows XRD patterns and photographs of composite films synthesized on a *c*-cut sapphire substrate. The films were translucent. The XRD patterns were indexed to the TAP (ICSD No. 98302), TAG (ICSD No. 33602), and α-Al_2O_3 (ICSD No. 130948) phases. Because only the diffraction peaks on the same plane as the substrate were measured for α-Al_2O_3, the

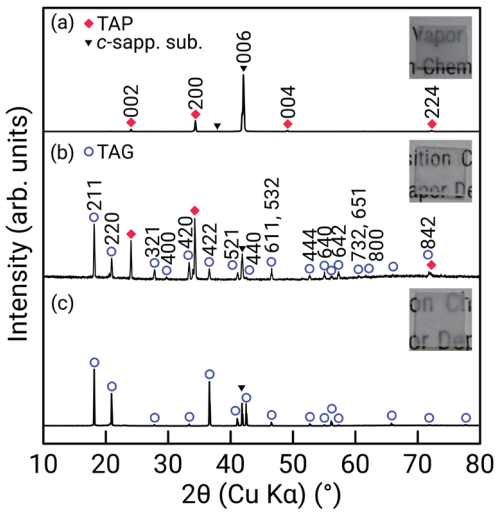

Fig. 1. (Color online) XRD patterns and photographs of the films prepared on *c*-cut sapphire substrate at various compositions: (a) 7.7, (b) 13.9, and (c) 27.0 mol%Tb_2O_3.

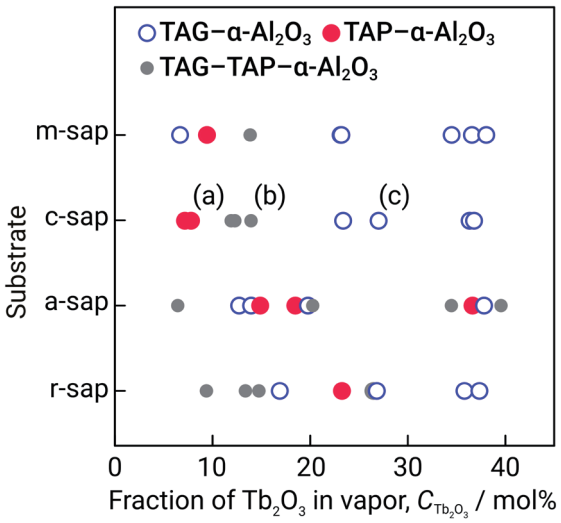

Fig. 2. (Color online) Phase mapping of the films prepared on *m*-, *c*-, *a*-, and *r*-cut sapphire substrates as a function of Tb_2O_3 molar ratio in precursor vapor. (a), (b), and (c) correspond to the XRD patterns in Fig. 1.

α-Al_2O_3 phase within the composite film exhibited homoepitaxial growth relative to the substrate. Figure 2 shows the phase mapping of the obtained films. The TAP–α-Al_2O_3 (filled circle) and TAG–α-Al_2O_3 (open circle) composite films tended to form on the Tb-poor and Tb-rich sides of the eutectic point (22.0 mol%Tb_2O_3), respectively. In some films, it was a three-phase mixed-phase film (gray-filled circle). Although the TAP and α-Al_2O_3 phases tended to form on the Al-rich side and the TAG and α-Al_2O_3 phases tended to form on the Tb-rich side, differences in the obtained phases on each plane of the sapphire substrate might be likely affected by differences between the composition in the precursor vapor and the composition within the film or by lattice matching between the substrate plane and each TAP and TAG phase.

Figure 3 shows SEM-BEI images of the composite films prepared on a *c*-cut sapphire substrate at various compositions. The light and dark gray areas correspond to the TAG or TAP phase and the α-Al_2O_3 phase, respectively. Composite films were formed in the range of 6.4–39.6 mol%Tb_2O_3, with film thicknesses of 1.51–9.16 μm. Deposition rates of the films were 9.1–55.0 μm h^{-1}. Figure 4 shows the structural mapping of the composite films prepared on various substrates. At compositions close to the eutectic point of 22.0 mol%Tb_2O_3, a lamellar structure formed (light- and dark-gray-filled squares in Fig. 4), while at compositions far from the eutectic point, a rod-like structure formed (open and filled squares in Fig. 4). On the Tb-poor side of the eutectic point, TAP and TAG were dispersed in the α-Al_2O_3 matrix, whereas on the Tb-rich side, α-Al_2O_3 was dispersed in the TAP and TAG matrix. Some films had a fine particulate dispersed structure formed within the grown grains (triangles in Fig. 4).

Figures 5(a) and 5(b) show the PLE and PL spectra of the TAP–α-Al_2O_3 and TAG–α-Al_2O_3 composite films prepared on a *c*-plane sapphire substrate at 7.7 and 27.0 mol%Tb_2O_3,

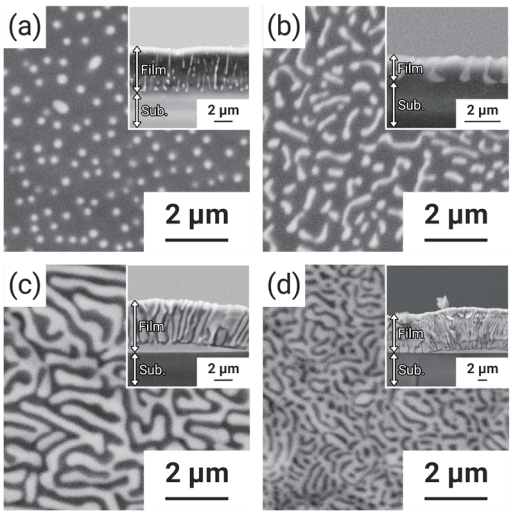

Fig. 3. Surface SEM-BEI images of the films prepared on *c*-cut sapphire substrate: (a) TAP–α-Al_2O_3 film (7.7 mol%Tb_2O_3), (b) TAP–TAG–α-Al_2O_3 film (13.9 mol%Tb_2O_3), (c) TAG–α-Al_2O_3 film (27.0 mol%Tb_2O_3), and (d) TAG–α-Al_2O_3 film (36.3 mol%Tb_2O_3). The light and dark areas correspond to the TAP or TAG phase and the α-Al_2O_3 phase, respectively. Insets show the corresponding cross-sectional images.

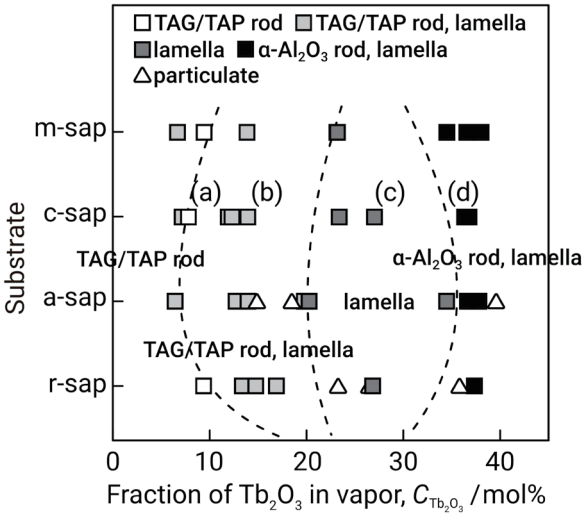

Fig. 4. Structural mapping of the films prepared on *m*-, *c*-, *a*-, and *r*-cut sapphire substrates as a function of Tb_2O_3 molar ratio in precursor vapor: TAG/TAP rod in α-Al_2O_3 matrix (open square), TAG/TAP rod and lamella in α-Al_2O_3 matrix (light-gray-filled square), lamella (dark-gray-filled square), α-Al_2O_3 rod and lamella in TAG/TAP matrix (filled matrix), and particulate dispersed structure (triangle). (a)–(d) correspond to the SEM images in Fig. 3.

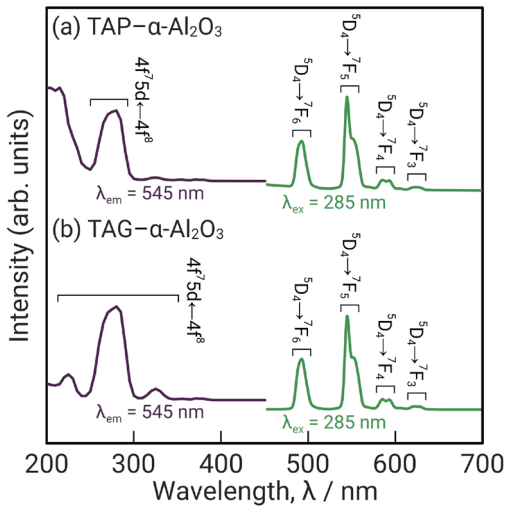

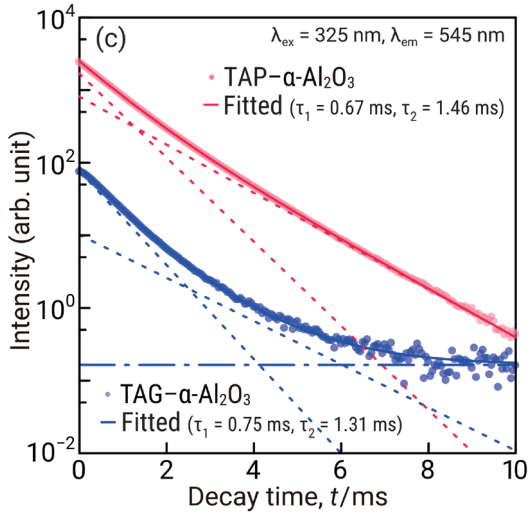

Fig. 5. (Color online) PLE spectrum monitored at 545 nm and PL spectrum excited at 325 nm for (a) TAP–α-Al_2O_3 composite film prepared on *c*-cut sapphire substrate at 7.7 mol%Tb_2O_3 and (b) TAG–α-Al_2O_3 composite film prepared on *c*-cut sapphire substrate at 27.0 mol%Tb_2O_3. (c) Afterglow decay profiles monitored at 545 nm and excited at 325 nm of the corresponding TAP– and TAG–α-Al_2O_3 composite films. Solid lines indicate the total fitting curves with bi-component exponential function.

respectively. The PLE peaks in the wavelength range of 200–350 nm were attributed to the transition of the $4f^8$ level to the $4f^75d$ level of Tb^{3+} centers in the TAP, TAG, and α-Al_2O_3 phases.[22–24] The PLE absorption at 230 nm was prominent for Tb^{3+} in the α-Al_2O_3 phase, suggesting that Tb^{3+} was solid-solved in the α-Al_2O_3 phase of the TAP-α-Al_2O_3 films. The PL peaks in the wavelength range of 450–650 nm were associated with the transition of the $^5D_4$ level to the ^7F_n (n = 3–6) levels of Tb^{3+} centers in the TAP, TAG, and α-Al_2O_3 phases.[23–27] The PL spectra were nearly identical regardless of the substrate plane and microstructure. This might be because the peak position of the f-f transition of Tb^{3+} is less susceptible to the effect of the coordination environment. Figure 5(c) shows the afterglow decay curves of the corresponding TAP–α-Al_2O_3 and TAG–α-Al_2O_3 composite films measured at 545 nm and excited at 325 nm. The measured decay curves were fitted with a bi-component exponential function:

$$I(t) = A_1\exp(-t/\tau_1) + A_2\exp(-t/\tau_2) + C, \quad (1)$$

where t is the decay time, A_1 and A_2 are constants, τ_1 and τ_2 are decay time constants, and C is a constant for baseline (if needed). τ_1 and τ_2 were determined to be 0.67 and 1.46 ms for the TAP–α-Al_2O_3 composite film and 0.75 and 1.31 ms for the TAG–α-Al_2O_3 composite film, respectively, using the Fityk software.[28]

Onishi *et al.* studied the decay curves of Tb^{3+} in the TAP, TAG, and α-Al_2O_3 phases measured at 545 nm with a tri-component exponential function, and they reported that the decay time constants were 0.0039, 0.02, and 0.53 ms for the Tb^{3+} center in the TAP phase,[22] 0.02, 0.1, and 1.3 ms for the Tb^{3+} center in the TAG phase,[23] and 0.06, 0.40, and 1.43 ms for the Tb^{3+} center in the α-Al_2O_3 phase.[24] Therefore, for the TAP–α-Al_2O_3 composite film, τ_1 = 0.67 ms was attributed to the Tb^{3+} centers in the TAP and α-Al_2O_3 phases and τ_2 = 1.46 ms corresponded to the Tb^{3+} center in the α-Al_2O_3 phase. For the TAG–α-Al_2O_3 composite film, τ_1 = 0.75 ms was attributed to the Tb^{3+} center in the α-Al_2O_3 phase and τ_2 = 1.31 ms arose from the Tb^{3+} centers in the α-Al_2O_3 and TAG phases.

4. Conclusions

We successfully synthesized TAP–α-Al_2O_3 and TAG–α-Al_2O_3 composite films by the LCVD method. The composite films had the lamellar structure at compositions close to the eutectic point, whereas the films showed the rod-like structure at compositions far from the eutectic point. The PLE peaks were associated with the transition of $4f^75d$ to $4f^8$ levels of the Tb^{3+} centers, and the emissions were associated with the transition of $^5D_4$ to ^7F_n (n = 3–6) levels of the Tb^{3+} centers. The decay time constants of the TAP–α-Al_2O_3 films were 0.67 and 1.46 ms, and those of the TAG–α-Al_2O_3 films were 0.75 and 1.31 ms. Those values were attributed to the Tb^{3+} centers in the TAP, TAG, and α-Al_2O_3 phases.

Acknowledgments

This study was supported in part by JSPS KAKENHI Grant Numbers 21H05199, 24K91211, 24K21685, 24K21746, and 25H00796.

References

1 Y. Waku, N. Nakagawa, T. Wakamoto, H. Ohtsubo, K. Shimizu, and Y. Kohtoku: Nature **389** (1997) 49. https://doi.org/10.1038/37937
2 Y. Waku, N. Nakagawa, T. Wakamoto, H. Ohtsubo, K. Shimizu, and Y. Kohtoku: J. Mater. Sci. **33** (1998) 4943. https://doi.org/10.1023/A:1004486303958
3 Y. Waku, N. Nakagawa, H. Ohtsubo, A. Mitani, and K. Shimizu: J. Mater. Sci. **36** (2001) 1585. https://doi.org/10.1023/A:1017519113164
4 A. Yoshikawa, K. Hasegawa, J. H. Lee, S. D. Durbin, B. M. Epelbaum, D. H. Yoon, T. Fukuda, and Y. Waku: J. Cryst. Growth **218** (2000) 67. https://doi.org/10.1016/S0022-0248(00)00516-9
5 E. Mihóková, M. Nikl, J. A. Mareš, A. Beitlerová, A. Vedda, K. Nejezchleb, K. Blažek, and C. D'Ambrosio: J. Lumin. **126** (2007) 77. https://doi.org/10.1016/j.jlumin.2006.05.004
6 Q. Sai, Z. Zhao, C. Xia, X. Xu, F. Wu, J. Di, and L. Wang: Opt. Mater. **35** (2013) 2155. https://doi.org/10.1016/j.optmat.2013.05.035
7 A. Shakhno, T. Zorenko, S. Witkiewicz-Łukaszek, M. Cieszko, Z. Szczepański, O. Vovk, S. Nizhankovskyi, Y. Siryk, and Y. Zorenko: Materials **16** (2023) 2701. https://doi.org/10.3390/ma16072701
8 Y. Ohashi, N. Yasui, Y. Yokota, A. Yoshikawa, and T. Den: Appl. Phys. Lett. **102** (2013) 051907. https://doi.org/10.1063/1.4790295
9 A. Yoshikawa, K. Kamada, S. Kurosawa, Y. Yokota, A. Yamaji, V. I. Chani, Y. Ohashi, and M. Yoshino: J. Cryst. Growth **498** (2018) 170. https://doi.org/10.1016/j.jcrysgro.2018.02.032
10 K. Kamada, H. Yamaguchi, N. Yasui, R. Ohashi, T. Den, K. J. Kim, M. Yoshino, A. Yamaji, S. Kurosawa, Y. Shoji, Y. Yokota, Vladimir. V. Kochurikhin, and A. Yoshikawa: Jpn. J. Appl. Phys. **60** (2021) SBBK04. https://doi.org/10.35848/1347-4065/abd708
11 C. He, Q. Sai, C. Xia, and H. Hu: Cryst. Res. Technol. **52** (2017) 1700056. https://doi.org/10.1002/crat.201700056
12 C. Deng, C. He, Q. Sai, Y. Liu, C. Xia, and X. Gu: Optik **160** (2018) 176. https://doi.org/10.1016/j.ijleo.2018.01.093
13 L. Sun, C. Zhou, T. Du, Z. Wu, Y. Lei, J. Li, H. Su, and J. Wang: J. Inorg. Mater. **36** (2021) 652. https://doi.org/10.15541/jim20200508
14 H. Su, J. Zhang, C. Cui, L. Liu, and H. Fu: J. Alloys Compd. **456** (2008) 518. https://doi.org/10.1016/j.jallcom.2007.04.026
15 J. Zhang, H. Su, B. Tang, L. Liu, and H. Fu: J. Cryst. Growth **310** (2008) 490. https://doi.org/10.1016/j.jcrysgro.2007.10.054
16 A. Ito, Y. You, T. Ichikawa, K. Tsuda, and T. Goto: J. Eur. Ceram. Soc. **34** (2014) 155. https://doi.org/10.1016/j.jeurceramsoc.2013.07.025
17 S. Matsumoto and A. Ito: J. Ceram. Soc. Jpn. **129** (2021) 1. https://doi.org/10.2109/jcersj2.20156
18 Y. Mitsuhashi, S. Matsumoto, and A. Ito: J. Am. Ceram. Soc. **106** (2023) 5140. https://doi.org/10.1111/jace.19176
19 S. Matsumoto, S. Kurosawa, D. Yokoe, T. Kimura, and A. Ito: Opt. Mater. **138** (2023) 113674. https://doi.org/10.1016/j.optmat.2023.113674
20 S. Matsumoto, A. Minamino, and A. Ito: Sens. Mater. **33** (2021) 2209. https://doi.org/10.18494/SAM.2021.3325
21 A. Ito, H. Kadokura, T. Kimura, and T. Goto: J. Alloys Compd. **489** (2010) 469. https://doi.org/10.1016/j.jallcom.2009.09.088
22 Y. Onishi, T. Nakamura, H. Sone, and S. Adachi: Jpn. J. Appl. Phys. **57** (2018) 082601. https://doi.org/10.7567/JJAP.57.082601
23 Y. Onishi, T. Nakamura, and S. Adachi: J. Lumin. **183** (2017) 193. https://doi.org/10.1016/j.jlumin.2016.11.035
24 Y. Onishi, T. Nakamura, and S. Adachi: Jpn. J. Appl. Phys. **55** (2016) 112401. https://doi.org/10.7567/JJAP.55.112401
25 Yu. V. Zorenko and V. I. Gorbenko: Phys. Solid State **51** (2009) 1800. https://doi.org/10.1134/S1063783409090078
26 Y. Hashimoto and A. Ito: Mater. Lett. **366** (2024) 136558. https://doi.org/10.1016/j.matlet.2024.136558
27 D. Nakauchi, T. Kato, N. Kawaguchi, and T. Yanagida: Sens. Mater. **33** (2021) 2203. https://doi.org/10.18494/SAM.2021.3323
28 M. Wojdyr: J. Appl. Crystallogr. **43** (2010) 1126. https://doi.org/10.1107/S0021889810030499